A Robust Deadbeat Predictive Controller With Delay Compensation Based on Composite Sliding-Mode Observer for PMSMs

Xiaodong Sun, *Senior Member, IEEE*, Junhao Cao, Gang Lei, *Member, IEEE*, Youguang Guo, *Senior Member, IEEE*, and Jianguo Zhu, *Senior Member, IEEE*

***Abstract*—This article proposes an improved deadbeat predictive controller for permanent-magnet synchronous motor drive systems. It can eliminate the influence of the parameter mismatch of inductance, resistance, and flux linkage. First, the performance of the conventional predictive current method is investigated to analyze sensitivities of the electric parameters. Then, a composite sliding-mode disturbance observer (SMDO) based on the stator current and lumped disturbance is proposed, which can simultaneously estimate the future current value and lumped disturbance caused by the parameter mismatch of inductance, resistance, and flux linkage. Based on the discrete-time SMDO, currents are estimated and used to replace the sampled values to compensate one-step delay caused by the calculation and sampling delay. Both simulation and experimental performances of the proposed method have been validated and compared with the conventional control methods under different conditions. The comparison results show the superiority of the proposed predictive current control method based on the composite SMDO.**

***Index Terms*—Deadbeat predictive control (DBPC), permanent-magnet synchronous motor (PMSM), sensitivity, sliding-mode disturbance observer (SMDO).**

I. Introduction

A. Motivation

DUE to the inherent features of high efficiency, high power density, and fast control response, permanent-magnet synchronous motors (PMSMs) have been widely applied in electric vehicles [1]–[5]. The classical field-oriented control (FOC) has been widely adopted in the PMSM drive system to achieve the desired servo control performance for its effective and reliable control methodology [6]–[8].

In FOC-based PMSM drive control, a double cascade loop controller is typically employed. High-performance electrical drives require efficient inner current control loops due to the intrinsic relationship between the current quality response and torque control. In order to achieve high transient performance and steady-state precision, many current control schemes have been investigated, including proportional–integral control [9], hysteresis control [10], and predictive control [11]–[13].

Among them, the predictive control has coherent and advantageous characteristics, such as improved rotational speed response. The main principle of the predictive control is to predict the future behavior of the state variables through a drive system model [14]–[16]. In addition, hysteresis-based, trajectory-based, deadbeat predictive control (DBPC), and finite-set model predictive control are known as the main four types of the predictive control, which are applied to the motor control. Among them, the DBPC and model predictive control are the most widely researched predictive control schemes [17], [18].

B. Related Research

Model predictive control can predict the future behavior of the states through the system discrete model and inherent discrete characteristics of an inverter. Then, it determines the future voltage vector based on the optimization of the cost function. The selected voltage vector is one of the seven basic voltage vectors and can minimize the cost function, which is used for the output of the control system. Model predictive control has good ability to handle the constraints of system variables, such as the maximum output voltage limits from the inverter. Furthermore, the advantages of robustness ensure that the model predictive control provides excellent control of the overall system performance. However, an inevitable drawback of the model predictive control is that the switching frequency may vary, as the state of switches depends on the sequence of inputs, leading to a suboptimal current ripple [19]–[22].

Compared with the model predictive control and other predictive control approaches, the DBPC combines good dynamic performance with constant switching frequency, which can force

Manuscript received June 22, 2020; revised August 13, 2020, December 9, 2020, and January 18, 2021; accepted February 23, 2021. Date of publication March 2, 2021; date of current version June 1, 2021. This work was supported in part by the National Natural Science Foundation of China under Project 51875261, in part by the Natural Science Foundation of Jiangsu Province of China under Project BK20180046, in part by the "Qinglan Project" of Jiangsu Province, and in part by the Postgraduate Research and the Practice Innovation Program of Jiangsu Province under Project SJCX19_0574. Recommended for publication by Associate Editor T. Dragicevic. *(Corresponding author: Gang Lei.)*

Xiaodong Sun and Junhao Cao are with the Automotive Engineering Research Institute, Jiangsu University, Zhenjiang 212013, China (e-mail: xdsun@ujs.edu.cn; caojunhaoujs@163.com).

Gang Lei and Youguang Guo are with the School of Electrical and Data Engineering, University of Technology Sydney, Sydney, NSW 2007, Australia (e-mail: gang.lei@uts.edu.au; youguang.guo-1@uts.edu.au).

Jianguo Zhu is with the School of Electrical and Information Engineering, University of Sydney, Sydney, NSW 2006, Australia (e-mail: jianguo.zhu@sydney.edu.au).

Color versions of one or more figures in this article are available at https://doi.org/10.1109/TPEL.2021.3063226

Digital Object Identifier 10.1109/TPEL.2021.3063226

the control error to zero in a short time. Thus, DBPC has been widely used in many applications, including pulsewidth modulation (PWM) rectifiers, active filter control [23], and motor drive control [24]. Since the DBPC does not need a cost function minimization algorithm, it is less computationally complex than the model predictive control [25]–[27]. The method forecasts voltage reference values based on the motor discrete model and then converts them into corresponding switch configurations by a space vector PWM. Based on the above-mentioned idea, the DBPC includes predictive current control and deadbeat (DB) control direct torque control. The accurate current control with working flux estimation may still lead to inaccurate torque control of the motor, which results in the adoption of DB direct torque control. In [28], an advanced DB direct torque and flux control strategy was proposed to improve the operation performance in which a decouple control strategy of torque and stator flux was proposed by constructing the algorithm model in the stator flux oriented coordinate system, which shows superiority in torque control.

Both transient and steady-state performances of the DBPC method crucially depend on the accuracy of the stator resistance, inductance, as well as permanent-magnet flux-linkage parameter. However, the electric parameters, including flux linkage, resistance, and inductance, may change due to the temperature rise and magnetic saturation, especially under the high-temperature operation conditions [29]. In [19], a new discrete-time robust predictive current controller was presented for PMSM drives in which a discrete-time integral term is added to the DB current prediction to provide the robustness against norm bounded parametric uncertainties and unmodeled dynamics. In [30], a composite control method combining DB predictive current control part and the current prediction and feedforward compensation part was proposed to promote control performance. In the designed stator current and disturbance observer, a novel sliding-mode exponential reaching law was introduced to further suppress the chattering of the observer. The composite control method is a creative DB current control method, which solves the parameters mismatch problem through a feedforward compensation part and further suppresses the chattering of voltage compensation significantly. However, there are still some problems with the reference. The performance of the sliding-mode disturbance observer (SMDO) is dependent on the design of the new approach law, which requires a smaller reaching time and sliding-mode ripples. Additionally, it is necessary to make a reasonable balance between the computational load caused by the design of the complex reaching law and the performance of the law. Due to the digital implementation of the predictive control, computing and sampling delay is inevitable [31]. However, the reference does not consider the delay in controller design, which will lead to the system performance degradation.

In order to overcome the above-mentioned problems, some methods have been proposed. In [21], a robust high-bandwidth discrete-time predictive current control scheme for the voltage-source pulsewidth-modulated converters was presented in which a digital predictive current controller with delay compensation is adopted based on a current observer with an adaptive internal model. In [32], an oversampling DB current control approach was presented to achieve a constant switching frequency and an optimal current ripple along with a high-current loop bandwidth and robust behavior to parameter variation. In [33], a robust predictive current control was proposed to eliminate the influence of inductance parameter mismatch. However, the influence caused by the mismatch of the permanent-magnet flux linkage and resistance is ignored. In [34], an improved DB-based predictive current control scheme based unified high-order sliding-mode disturbance observer was proposed to promote speed robustness and current tracking accuracy. It is a creative DB control method, which essentially solves the mismatch problem of mechanical and electrical parameters through disturbance compensation with feedback to the designed control system.

C. Contributions

An improved DB predictive controller is developed to guarantee the performance of PMSM drives regardless of the parameter mismatch and one-step delay in digital control in this work. Compared with the conventional predictive current controller, the proposed method can achieve lower control currents' ripples based on the current and lumped disturbance discrete-time sliding-mode observer (SMO). Furthermore, the compensation of calculation time delay is considered and the second-order expansion of the rotor speed is adopted to improve the current reference accuracy.

The main contributions of this article are listed as follows.

1) This article proposes a different disturbance observer to be applied in the improved DB predictive current controller, which is designed through analyzing the structure of the current state-space equations to effectively eliminate the coupling terms. Therefore, the design idea is completely different from the high-order sliding-mode structure or new reaching law-based method in the mentioned references.
2) The design method based on the state-space structure of the control plant reduces the calculation complexity of the observation value for the nonlinear model, which is conducive to achieve higher control accuracy.
3) In order to suppress the influence of the control delay, one-step delay compensation is considered to calculate the voltage vector $u_{dq}(k+1)$. Furthermore, the compensation inevitably causes a two-sample delay in the reference tracking of the reference currents $i^*_{dq}(k)$, which can be ignored by the appropriate design of control parameters.
4) In order to improve the current reference accuracy, the second-order expansion of the rotor speed is adopted in the method, which further improves the control performance.

The remainder of this article is organized as follows. Section II describes the mathematical model of a surface-mounted PMSM (SPMSM) and develops the model under parameter disturbance. In Section III, based on the discrete-time model of the SPMSM, parameter sensitivity of the conventional predictive current control to inductance, resistance, and flux linkage is analyzed. In Section IV, a discrete-time SMDO based on the stator current

and disturbance is designed to eliminate the influence of parameter mismatch and compensate one-step delay. The simulation and experimental results are provided in Section V. Finally, Section VI gives the summary and draws the conclusion of the article.

II .Mathematical Model

The dynamical model of the SPMSM can be described in the *dq* synchronously rotating reference frame as follows:

$$\begin{cases} u_d = R_s i_d + \frac{d\psi_d}{dt} - \omega_e \psi_q \\ u_q = R_s i_q + \frac{d\psi_q}{dt} + \omega_e \psi_d. \end{cases} \tag{1}$$

The flux-linkage equation is

$$\begin{cases} \psi_d = L_d i_d + \psi_f \\ \psi_q = L_q i_q \end{cases} \tag{2}$$

where u_d, u_q, i_d, and i_q are the d- and q-axis components of the stator voltage and current, respectively. R_s and L_s represent the stator resistance and inductance, respectively, ψ_f is the permanent-magnet flux linkage, and ω_e is the electrical angular speed.

The system model can be written in the standard state-space form as

$$\frac{d}{dt}\begin{bmatrix} i_d \\ i_q \end{bmatrix} = \boldsymbol{P} \cdot \begin{bmatrix} i_d \\ i_q \end{bmatrix} + \boldsymbol{Q} \cdot \begin{bmatrix} u_d \\ u_q \end{bmatrix} + \begin{bmatrix} 0 \\ -\omega_e \psi_f / L_s \end{bmatrix} \tag{3}$$

where $\boldsymbol{P} = \left[\begin{smallmatrix} -R_s/L_s & \omega_e \\ -\omega_e & -R_s/L_s \end{smallmatrix}\right]$ and $\boldsymbol{Q} = \left[\begin{smallmatrix} 1/L_s & 0 \\ 0 & 1/L_s \end{smallmatrix}\right]$.

The electromagnetic torque and mechanical equations of SPMSM are shown as follows:

$$\begin{cases} T_e = \frac{3}{2} p_n \psi_f i_q \\ \frac{J}{p_n}\frac{d\omega_e}{dt} = T_e - T_L \end{cases} \tag{4}$$

where J is the moment of inertia, p_n is the number of pole pairs, and T_e and T_L are the electromagnetic torque and the load torque, respectively.

According to (3) and (4), when the mismatch of three machine parameters exists, the dynamical model can be written as

$$\begin{cases} \frac{di_d}{dt} = -\frac{\tilde{R}_s}{\tilde{L}_s} i_d + \omega_e i_q + \frac{1}{\tilde{L}_s} u_d + r_d \\ \frac{di_q}{dt} = -\frac{\tilde{R}_s}{\tilde{L}_s} i_q - \omega_e i_d + \frac{1}{\tilde{L}_s} u_q - \frac{\tilde{\psi}_f \omega_e}{\tilde{L}_s} + r_q \\ \frac{d\omega_e}{dt} = \frac{3{p_n}^2 \tilde{\psi}_f}{2J} i_q + r_{\omega_e} \end{cases} \tag{5}$$

where r_d, r_q, and r_{ω_e} represent the parameter perturbances, which consist of the flux-linkage error, resistance error, and induction error, respectively. And the perturbances can be described as

$$\begin{cases} r_d = \frac{-\Delta L_s \tilde{R}_s + L_s \Delta \tilde{R}_s}{\tilde{L}_s\left(\tilde{L}_s - \Delta L_s\right)} i_d + \frac{\Delta L_s}{\tilde{L}_s\left(\tilde{L}_s - \Delta L_s\right)} u_d \\ r_q = \frac{-\Delta L_s \tilde{R}_s + \tilde{L}_s \Delta R_s}{\tilde{L}_s\left(\tilde{L}_s - \Delta L_s\right)} i_q + \frac{\Delta L_s}{\tilde{L}_s\left(\tilde{L}_s - \Delta L_s\right)} u_q \\ \qquad + \frac{-\Delta L_s \tilde{\psi}_f + \tilde{L}_s \Delta \psi_f}{\tilde{L}_s\left(\tilde{L}_s - \Delta L_s\right)} \omega_e \\ r_{\omega_e} = -\frac{3{p_n}^2 \Delta \psi_f}{2J} i_q - \frac{p_n}{J} T_L. \end{cases} \tag{6}$$

And $\tilde{R}_s = R_s + \Delta R_s$, $\tilde{L}_s = L_s + \Delta L_s$, and $\tilde{\psi}_f = \psi_f + \Delta\psi_f$ are the nominal values of system parameters. ΔR_s, ΔL_s, and $\Delta\psi_f$ are the parameters errors between the nominal values and the actual values.

III. Parameter Sensitivity Analysis

A. Conventional DBPC Method

In order to digitally implement the model-based controller, the discretization of the plant equations is necessary. The discretized state-space form of the plant (3) around a generic time instant k is presented as

$$\begin{bmatrix} i_d(k+1) \\ i_q(k+1) \end{bmatrix} = \boldsymbol{M}(k) \cdot \begin{bmatrix} i_d(k) \\ i_q(k) \end{bmatrix} + \boldsymbol{N} \cdot \begin{bmatrix} u_d(k) \\ u_q(k) \end{bmatrix} + \boldsymbol{T}(k) \tag{7}$$

where

$$\boldsymbol{M}(k) = e^{\boldsymbol{P}T_s}, \quad \boldsymbol{N} = \int_0^{T_s} e^{\boldsymbol{P}t}\boldsymbol{Q}dt$$

$$\boldsymbol{T}(k) = \begin{bmatrix} 0 \\ -\omega_e(k)\psi_f T_s / L_s \end{bmatrix}$$

and T_s denotes the sampling period of the control system.

Taylor expansion is carried out on $\boldsymbol{M}$ and $\boldsymbol{N}$, and the quadratic and higher order terms are ignored. Then, the matrices of the state-space model are as follows:

$$\boldsymbol{M}(k) = \begin{bmatrix} 1 - T_s R_s / L_s & T_s \omega_e(k) \\ -T_s \omega_e(k) & 1 - T_s R_s / L_s \end{bmatrix}$$

$$\boldsymbol{N} = \begin{bmatrix} T_s / L_s & 0 \\ 0 & T_s / L_s \end{bmatrix}.$$

According to (7), the output voltage vector of the DBPC is expressed as follows:

$$\begin{bmatrix} u_d(k) \\ u_q(k) \end{bmatrix} = \boldsymbol{N}^{-1} \left\{ \begin{bmatrix} i_d^*(k+1) \\ i_q^*(k+1) \end{bmatrix} - \boldsymbol{M}(k) \cdot \begin{bmatrix} i_d(k) \\ i_q(k) \end{bmatrix} - \boldsymbol{T}(k) \right\} \tag{8}$$

where $i_d^*(k+1)$ and $i_q^*(k+1)$ are the reference currents in the *dq* axes reference rotor frame. It can be seen that the future reference current value $i^*(k+1)$ is needed, which can be assumed to be equal to the actual value $i^*(k)$, for T_s is short enough compared with the dynamic behavior of the system. Therefore, the reference current value can be considered constant over T_s.

The output stator voltage vector enables the actual current vector to approach the expected values. The block diagram of the conventional DBPC is illustrated in Fig. 1. The voltage vector is obtained through the predictive mode (8), which is converted to switching signals through the modulation process.

B. Parameter Sensitivity Analysis

The DBPC is a predictive control method based on the mathematical model of PMSM due to the existence of three machine parameters in a current prediction model. This means that the DB predictive controller is subject to parameter sensitivity, and the accuracy of the prediction model will directly influence the control performance. In order to evaluate the relationship

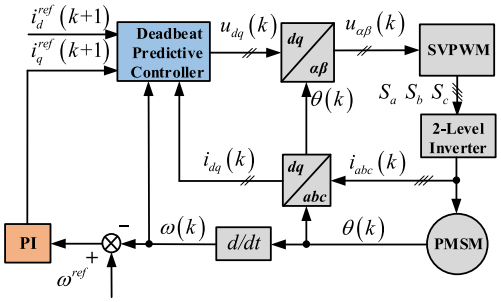

Fig. 1. Block diagram of the conventional DBPC.

between the prediction error and three parameters mismatch, the parameter sensitivity analysis is discussed.

According to (7), the discrete current model under the parameters disturbance can be expressed as follows:

$$\begin{bmatrix} \tilde{i}_d(k+1) \\ \tilde{i}_q(k+1) \end{bmatrix} = \tilde{\boldsymbol{M}}(k) \cdot \begin{bmatrix} i_d(k) \\ i_q(k) \end{bmatrix} + \tilde{\boldsymbol{N}} \cdot \begin{bmatrix} u_d(k) \\ u_q(k) \end{bmatrix} + \tilde{\boldsymbol{T}}(k) \tag{9}$$

where

$$\tilde{\boldsymbol{M}}(k) = \begin{bmatrix} 1 - T_s\tilde{R}_s/\tilde{L}_s & T_s\omega_e(k) \\ -T_s\omega_e(k) & 1 - T_s\tilde{R}_s/\tilde{L}_s \end{bmatrix}$$

$$\tilde{\boldsymbol{N}} = \begin{bmatrix} T_s/\tilde{L}_s & 0 \\ 0 & T_s/\tilde{L}_s \end{bmatrix}, \quad \tilde{\boldsymbol{T}}(k) = \begin{bmatrix} 0 \\ -\omega_e(k)\tilde{\psi}_f T_s/\tilde{L}_s \end{bmatrix}.$$

Therefore, the errors between the current response values and the current reference values subjected to parameter perturbation can be obtained as

$$\begin{cases} e_d = \tilde{i}_d(k+1) - i_d(k+1) \\ e_q = \tilde{i}_q(k+1) - i_q(k+1) \end{cases} \tag{10}$$

with

$$\begin{cases} e_d = \frac{\Delta L_s R_s - L_s \Delta R_s}{L_s(\Delta L_s + L_s)} T_s i_d(k) - \frac{\Delta L_s}{L_s(\Delta L_s + L_s)} T_s u_d(k) \\ e_q = \frac{\Delta L_s R_s - L_s \Delta R_s}{L_s(\Delta L_s + L_s)} T_s i_q(k) - \frac{\Delta L_s}{L_s(\Delta L_s + L_s)} T_s u_q(k) \\ \quad + \frac{\Delta L_s \psi_f - L_s \Delta \psi_f}{L_s(\Delta L_s + L_s)} T_s \omega_e(k). \end{cases} \tag{11}$$

Differentiating (11) yields

$$\begin{cases} \frac{\partial e_d}{\partial \Delta L_s} = \frac{T_s[(R_s + \Delta R_s) i_d(k) - u_d(k)]}{(\Delta L_s + L_s)^2} \\ \frac{\partial e_q}{\partial \Delta L_s} = \frac{T_s[(R_s + \Delta R_s) i_q(k) - u_q(k) - \omega_e(k)(\psi_f + \Delta\psi_f)]}{(\Delta L_s + L_s)^2} \\ \frac{\partial e_d}{\partial \Delta R_s} = -\frac{T_s i_d(k)}{(\Delta L_s + L_s)}, \quad \frac{\partial e_q}{\partial \Delta R_s} = -\frac{T_s i_q(k)}{(\Delta L_s + L_s)} \\ \frac{\partial e_d}{\partial \Delta \psi_f} = 0, \quad \frac{\partial e_q}{\partial \Delta \psi_f} = -\frac{T_s \omega_e(k)}{(\Delta L_s + L_s)}. \end{cases} \tag{12}$$

Equations (11) and (12) indicate that the d-axis current is not affected by the flux-linkage error $\Delta\psi_f$, while the dq axes currents are under influence of the resistance error ΔR_s and inductance error ΔL_s. Therefore, the uncertainty of any system parameter will cause errors in the current response. Meanwhile, the current response errors and error variation rates are related to the mechanical parameters, speed and currents.

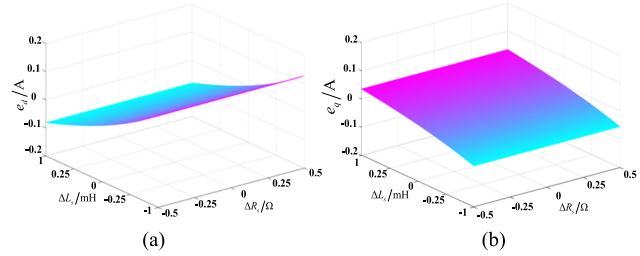

Fig. 2. Current prediction errors under inductance and resistance parameter mismatch. (a) d-axis current error. (b) q-axis current error.

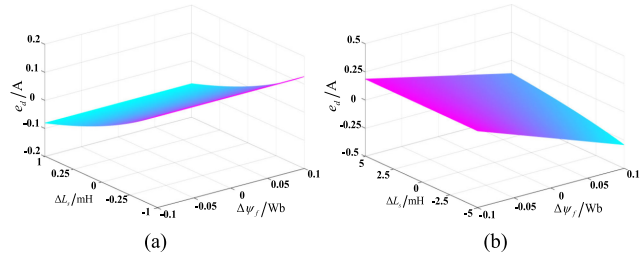

Fig. 3. Current prediction errors under inductance and flux-linkage parameter mismatch. (a) d-axis current error. (b) q-axis current error.

TABLE I
SPMSM AND SYSTEM PARAMETERS

Parameters	Symbol	Value
Number of pole pairs	P_n	22
Stator resistance	R_s	0.8 Ω
Stator inductance	L_s	4.5 mH
Permanent-magnet flux linkage	ψ_f	0.215 Wb
Inertia	J	0.03 kgm^2
Viscous friction coefficient	v	0.0006 N·m·s
Rated speed	N	360 rpm
Rated power	P_N	30 kW

The relationship of the dq axes current response errors and the parameter mismatch of inductance L_s, resistance R_s, and flux linkage ψ_f is shown in Figs. 2 and 3. The speed reference is set as 360 r/min and the load torque is set as 0. The SPMSM and system parameters are listed in Table I.

Fig. 2 shows the dq axes current response errors under inductance L_s and resistance R_s parameter mismatch. As shown, the resistance error has little effect on the dq axes current response errors when the parameter mismatch of inductance remains unchanged, while the inductance error has a great influence on the current prediction error. Fig. 3 illustrates the dq axes current prediction errors under the parameter mismatch of inductance L_s and flux linkage ψ_f. It can be seen that the parameter mismatch of flux linkage has no effect on the d-axis current response error. As shown in Fig. 3(b), the flux-linkage error produces remarkable influence on the q-axis current prediction errors.

According to the analysis above, the conclusion can be made that the conventional predictive current control method is sensitive to inductance, resistance, and flux-linkage parameters. Therefore, robustness design based on the predictive current controller should be considered.

IV. DBPC Method With Perturbance Observer

A. Composite SMDO Design

According to (5), the state equation can be expressed as follows when the parameter variations are taken into consideration:

$$\frac{d\boldsymbol{x}}{dt} = \boldsymbol{A}x + \boldsymbol{B}u + \boldsymbol{f}_a + \boldsymbol{f}_b \tag{13}$$

where

$$\boldsymbol{x} = \begin{bmatrix} i_d \\ i_q \\ \omega_e \end{bmatrix}, \boldsymbol{u} = \begin{bmatrix} u_d \\ u_q \\ i_{sq} \end{bmatrix}, \boldsymbol{f}_a = \begin{bmatrix} 0 \\ -\tilde{\psi}_f \omega_e / \tilde{L}_s \\ 0 \end{bmatrix}, \text{ and } \boldsymbol{f}_b = \begin{bmatrix} r_d \\ r_q \\ r_{\omega_e} \end{bmatrix}$$

are the state variables, system output, flux-linkage term, and lumped disturbance, respectively.

The coefficient matrices of the state equations are as follows:

$$\boldsymbol{A} = \begin{bmatrix} -\tilde{R}_s \big/ \tilde{L}_s & \omega_e & 0 \\ -\omega_e & -\tilde{R}_s \big/ \tilde{L}_s & 0 \\ 0 & 0 & 0 \end{bmatrix}$$

$$\boldsymbol{B} = \begin{bmatrix} 1 \big/ \tilde{L}_s & 0 & 0 \\ 0 & 1 \big/ \tilde{L}_s & 0 \\ 0 & 0 & 3{p_n}^2 \tilde{\psi}_f \big/ 2J \end{bmatrix}.$$

In order to implement the proposed DB predictive current controller, it is necessary to estimate the disturbance caused by the parameter variation. Since the SMO can estimate the uncertainty, the SMDO can be designed as follows based on (13):

$$\frac{d\hat{\boldsymbol{x}}}{dt} = \boldsymbol{A}\hat{\boldsymbol{x}} + \boldsymbol{B}u + \boldsymbol{f}_a + \boldsymbol{F}e + \boldsymbol{G}\mathrm{sgn}(\boldsymbol{e}) \tag{14}$$

where $\hat{\boldsymbol{x}}$ is the estimated value of state variables $\boldsymbol{x}$, sgn() is the symbolic function, and $\boldsymbol{F}$ and $\boldsymbol{G}$ are the gain matrices.

According to the sliding-mode control theory, the sliding-mode design procedure can be divided into two steps: the first step is the sliding-mode surface design, and the second step is to design the sliding-mode control function, which can force the state trajectory to converge to the sliding-mode surface. In this article, the sliding-mode surface is defined as

$$\boldsymbol{e} = \boldsymbol{x} - \hat{\boldsymbol{x}} = \begin{bmatrix} e_1 \\ e_2 \\ e_3 \end{bmatrix} = \begin{bmatrix} i_d - \hat{i}_d \\ i_q - \hat{i}_q \\ \omega_e - \hat{\omega}_e \end{bmatrix}. \tag{15}$$

According to (13) and (14), the error equation can be obtained as follows:

$$\frac{d\boldsymbol{e}}{dt} = \boldsymbol{A}e + \boldsymbol{f}_b - \boldsymbol{F}e - \boldsymbol{G}\mathrm{sgn}(\boldsymbol{e}) \tag{16}$$

where $\boldsymbol{F}$ and $\boldsymbol{G}$ are designed as follows:

$$\boldsymbol{F} = \begin{bmatrix} 0 & \omega_e & 0 \\ -\omega_e & 0 & 0 \\ 0 & 0 & 0 \end{bmatrix}, \quad \boldsymbol{G} = \begin{bmatrix} g_1 & 0 & 0 \\ 0 & g_2 & 0 \\ 0 & 0 & g_3 \end{bmatrix}.$$

In order to guarantee the convergence of current errors and disturbance estimation errors of the proposed composite SMDO, the Lyapunov candidate function is selected as follows:

$$\boldsymbol{V} = \frac{1}{2}\boldsymbol{e}^T\boldsymbol{e}. \tag{17}$$

Deriving (17) and combining with (16) yields

$$\begin{aligned} \frac{d\boldsymbol{V}}{dt} &= \boldsymbol{e}^T\left(\boldsymbol{A}e + \boldsymbol{f}_b - \boldsymbol{F}e - \boldsymbol{G}\mathrm{sgn}(\boldsymbol{e})\right) \\ &= \boldsymbol{e}^T\left(\boldsymbol{A} - \boldsymbol{F}\right)\boldsymbol{e} + \boldsymbol{e}^T\boldsymbol{f}_b - \boldsymbol{e}^T\boldsymbol{G}\mathrm{sgn}(\boldsymbol{e}). \end{aligned} \tag{18}$$

Substituting the gain matrices into (18) yields

$$\begin{aligned} \frac{d\boldsymbol{V}}{dt} = \boldsymbol{e}^T &\begin{bmatrix} -\tilde{R}_s \big/ \tilde{L}_s & 0 & 0 \\ 0 & -\tilde{R}_s \big/ \tilde{L}_s & 0 \\ 0 & 0 & 0 \end{bmatrix}\boldsymbol{e} + \boldsymbol{e}^T \begin{bmatrix} r_d \\ r_q \\ r_{\omega_e} \end{bmatrix} \\ &- \boldsymbol{e}^T \begin{bmatrix} g_1 & 0 & 0 \\ 0 & g_2 & 0 \\ 0 & 0 & g_3 \end{bmatrix} \mathrm{sgn}(\boldsymbol{e}). \end{aligned} \tag{19}$$

Simplifying (19), one can obtain the following:

$$\begin{aligned} &\frac{d\boldsymbol{V}}{dt} = -\frac{\tilde{R}_s}{\tilde{L}_s}e_1^2 - \frac{\tilde{R}_s}{\tilde{L}_s}e_2^2 + e_1 r_d + e_2 r_q + e_3 r_{\omega_e} - g_1\left|e_1\right| \\ &- g_2\left|e_2\right| - g_3\left|e_3\right| \\ &\le \left|e_1\right|\left(\left|r_d\right| - g_1\right) + \left|e_2\right|\left(\left|r_q\right| - g_2\right) + \left|e_3\right|\left(\left|r_{\omega_e}\right| - g_3\right) \\ &\le \left|e_1\right|\left(G_1 - g_1\right) + \left|e_2\right|\left(G_2 - g_2\right) + \left|e_3\right|\left(G_3 - g_3\right). \end{aligned} \tag{20}$$

Since the disturbance function is bounded, the boundary values are introduced, that is, the disturbance values satisfy $|r_d| < G_1$, $|r_q| < G_2$, and $|r_{\omega_e}| < G_3$. And the elements of the gain matrix $\boldsymbol{G}$ satisfy that $g_1 > G_1$, $g_2 > G_2$, and $g_3 > G_3$; then, the Lyapunov candidate function satisfies $dV/dt \le 0$. Therefore, the proposed SMDO with matrix $\boldsymbol{G}$ can reach the sliding-mode surface in finite time and remains stable, which ensures the asymptotic stability of the proposed composite SMDO and the parameter observations will approach the actual values.

B. Discrete Expression of Composite SMDO

As the proposed composite SMDO will be only computed with discrete form and applied to control system within the sampling period, it is necessary to deduce the discrete expression of the composite observer. Assuming that the sampling period is sufficiently small for the discrete-time system, the composite discrete-time observer can be discretized as (21) according to (14)

$$\begin{cases} \hat{i}_d(k+1) = \left(1 - \frac{T_s\tilde{R}_s}{\tilde{L}_s}\right)\hat{i}_d(k) \\ \quad + \frac{T_s}{\tilde{L}_s}u_d(k) + T_s\omega_e(k)\hat{i}_q(k) \\ \quad + T_s\hat{\omega}_e(k)e_2(k) + T_s g_1\mathrm{sgn}(e_1(k)) \\ \hat{i}_q(k+1) = \left(1 - \frac{T_s\tilde{R}_s}{\tilde{L}_s}\right)\hat{i}_q(k) + \frac{T_s}{\tilde{L}_s}u_q(k) \\ \quad - T_s\omega_e(k)\hat{i}_d(k) - \frac{T_s\tilde{\psi}_f}{L_s}\omega_e(k) \\ \quad - T_s\omega_e(k)e_1(k) + T_s g_2\mathrm{sgn}(e_2(k)) \\ \hat{\omega}_e(k+1) = \hat{\omega}_e(k) + \frac{3T_s{p_n}^2\tilde{\psi}_f}{2J}i_q(k) + T_s g_3\mathrm{sgn}(e_3(k)) \end{cases} \tag{21}$$

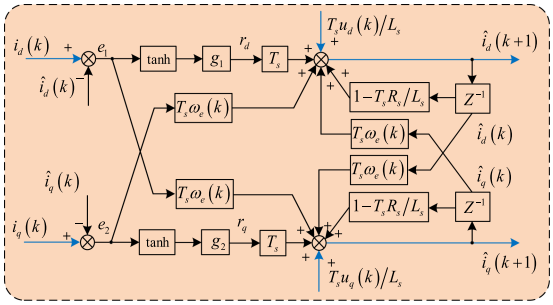

Fig. 4. Discrete block diagram of the proposed composite SMDO.

where $\hat{i}_d(k+1)$ and $\hat{i}_q(k+1)$ are the predictive values of the *dq* axes currents, and $\hat{\omega}_e(k+1)$ represents the predictive values of the electrical angular speed.

In order to suppress the predictive current ripple caused by a sign function, it is necessary to replace the sign function with a smoothing function, such as a hyperbolic tangent function with smooth continuity. Then, the discrete block diagram of the proposed composite SMDO is shown in Fig. 4.

When the system trajectory reaches the sliding-mode surface and enters the sliding-mode state, it can be obtained that

$$\frac{d\boldsymbol{e}}{dt} = \boldsymbol{e} = 0. \tag{22}$$

Combining the state equation of observer and (22) yields

$$\boldsymbol{f}_b = \boldsymbol{G}\tanh(\boldsymbol{e}). \tag{23}$$

Therefore, the variation rate of disturbance can be obtained as follows:

$$\begin{cases} r_d(k) = g_1\tanh(e_1(k)) \\ r_q(k) = g_2\tanh(e_2(k)) \\ r_{\omega_e}(k) = g_3\tanh(e_3(k)). \end{cases} \tag{24}$$

Combining (6) and (24), the estimated flux linkage can be obtained as

$$\Delta\psi_f(k) = \frac{2Jg_3\tanh(e_3(k)) + 2p_nT_L}{3{p_n}^2 i_q(k)}. \tag{25}$$

C. Predictive Current Control With Composite SMDO

According to (5) and (8), the discrete expression of the voltage equation can be described as

$$\begin{bmatrix} u_d(k) \\ u_q(k) \end{bmatrix} = \begin{bmatrix} i_d^*(k+1)\,\tilde{L}_s/T_s \\ i_q^*(k+1)\,\tilde{L}_s/T_s \end{bmatrix} - \begin{bmatrix} 0 \\ -\tilde{\psi}_f\omega_e(k) \end{bmatrix} - \tilde{L}_s\begin{bmatrix} r_d \\ r_q \end{bmatrix} - \begin{bmatrix} \tilde{L}_s/T_s - \tilde{R}_s & \tilde{L}_s\omega_e(k) \\ -\tilde{L}_s\omega_e(k) & \tilde{L}_s/T_s - \tilde{R}_s \end{bmatrix}\begin{bmatrix} i_d(k) \\ i_q(k) \end{bmatrix}. \tag{26}$$

When the control scheme based on the predictive current control is implemented experimentally, it is worth highlighting that the calculation and sampling delay is unavoidable due to the digital implementation mode of the prediction control. This delay can deteriorate the performance of the system if it is not considered in the design of the controller. In order to suppress the influence of the delay, it is necessary to calculate the voltage vector $u_{dq}(k+1)$ by using delay compensated currents $i_{dq}(k+1)$. Since the electromagnetic time constant is smaller than the mechanical time constant in the motor system, the rotor speed can be considered as constant during one sampling period. These compensated currents are employed to replace the measured currents $i_{dq}(k)$ of the model (26), which indicates that the voltage equation can be updated with one-step delay compensation as

$$\begin{bmatrix} u_d(k+1) \\ u_q(k+1) \end{bmatrix} = \begin{bmatrix} i_d^*(k+2)\,\tilde{L}_s/T_s \\ i_q^*(k+2)\,\tilde{L}_s/T_s \end{bmatrix} - \begin{bmatrix} 0 \\ -\tilde{\psi}_f\omega_e(k) \end{bmatrix} - \tilde{L}_s\begin{bmatrix} \hat{r}_d(k+1) \\ \hat{r}_q(k+1) \end{bmatrix} - \begin{bmatrix} \tilde{L}_s/T_s - \tilde{R}_s & \tilde{L}_s\omega_e(k) \\ -\tilde{L}_s\omega_e(k) & \tilde{L}_s/T_s - \tilde{R}_s \end{bmatrix}\begin{bmatrix} \hat{i}_d(k+1) \\ \hat{i}_q(k+1) \end{bmatrix}. \tag{27}$$

When the compensation of calculation time delay is considered, the future reference can be assumed to be $i_{dq}^*(k+2) = i_{dq}^*(k)$. The current reference approximation will lead to a two sampling delays in the reference tracking of the reference currents. Fortunately, the sampling time used, in this article, is small enough that the delay introduced by the approximation of future references can be ignored.

In order to improve the current reference accuracy, the second-order expansion of the rotor speed is adopted in the method, which is expressed as

$$\frac{\omega_e(k+1) - \omega_e(k)}{T} = \frac{d\omega_e}{dt} + \frac{d^2\omega_e}{dt^2}\cdot\frac{T}{2} \tag{28}$$

where T is the external loop sampling time, much larger than the sampling time T_s.

Combining (4) and (28) and considering the flux-linkage error, it can be obtained that

$$\frac{d^2\omega_e}{dt^2} = \frac{3{p_n}^2\left(\tilde{\psi}_f + \Delta\psi_f\right)}{2J}\frac{di_q}{dt}. \tag{29}$$

Substituting (4) and (29) into (28) yields

$$\frac{\omega_e(k+1) - \omega_e(k)}{T} = \frac{3{p_n}^2\left(\tilde{\psi}_f + \Delta\psi_f\right)}{2J}\frac{i_q(k) - i_q(k-1)}{2} + \frac{3{p_n}^2\left(\tilde{\psi}_f + \Delta\psi_f\right)}{2J}i_q(k) - \frac{p_n}{J}T_L. \tag{30}$$

The values for ω_e^* and $i_q^*(k)$ are used as the rotor speed and current reference in (30) by considering $\omega_e^* = \omega_e^*(k+1)$ and $i_q^*(k) = i_q(k)$.

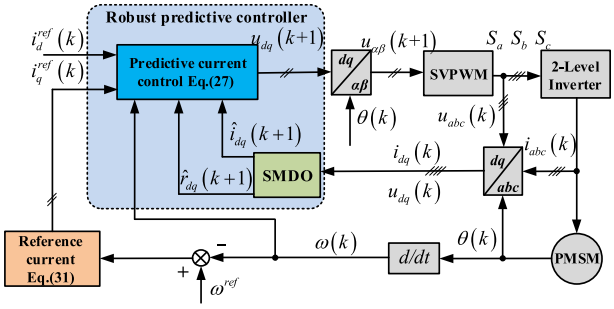

Fig. 5. Control diagram of the proposed DB predictive current controller.

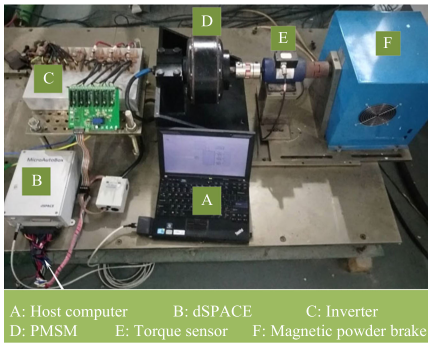

Fig. 6. Experimental setup used to verify the proposed DBPC method.

From (30), the reference current can be obtained as

$$i_q^*(k) = \frac{\begin{array}{c}4J\omega_e^* - 4J\omega_e(k) + 4Tp_nT_L \\ +3Tp_n{}^2\left(\tilde{\psi}_f + \Delta\psi_f(k)\right) i_q(k-1)\end{array}}{9Tp_n{}^2\left(\tilde{\psi}_f + \Delta\psi_f(k)\right)}. \quad (31)$$

The control diagram of the proposed DB predictive current controller is shown in Fig. 5. The proposed SMDO is used to compensate parameter disturbances with the estimated lumped disturbance value, which overcomes the influence of parameter mismatch on DBPC method. In order to reduce the influence of sampling and calculation due to the digital implementation of the control system, one-step delay is compensated.

V. Simulation and Experimental Results

For the purpose of verifying the effectiveness of the proposed method, simulations and experiments for comparison between the proposed method and the conventional DBPC have been conducted at a laboratory platform.

Simulations are established in MATLAB/Simulink. The experiments are performed on the platform of the dSPACE 1401 test bench through which the experimental measurements can be exported to MATLAB and plotted.

Since the parameters of the motor body cannot be set arbitrarily, the parameters in the control program are changed to achieve the corresponding parameter mismatch. The experimental setup consists of an SPMSM, a torque sensor, and a magnetic powder brake, as shown in Fig. 6. The parameters of the SPMSM system are listed in Table I.

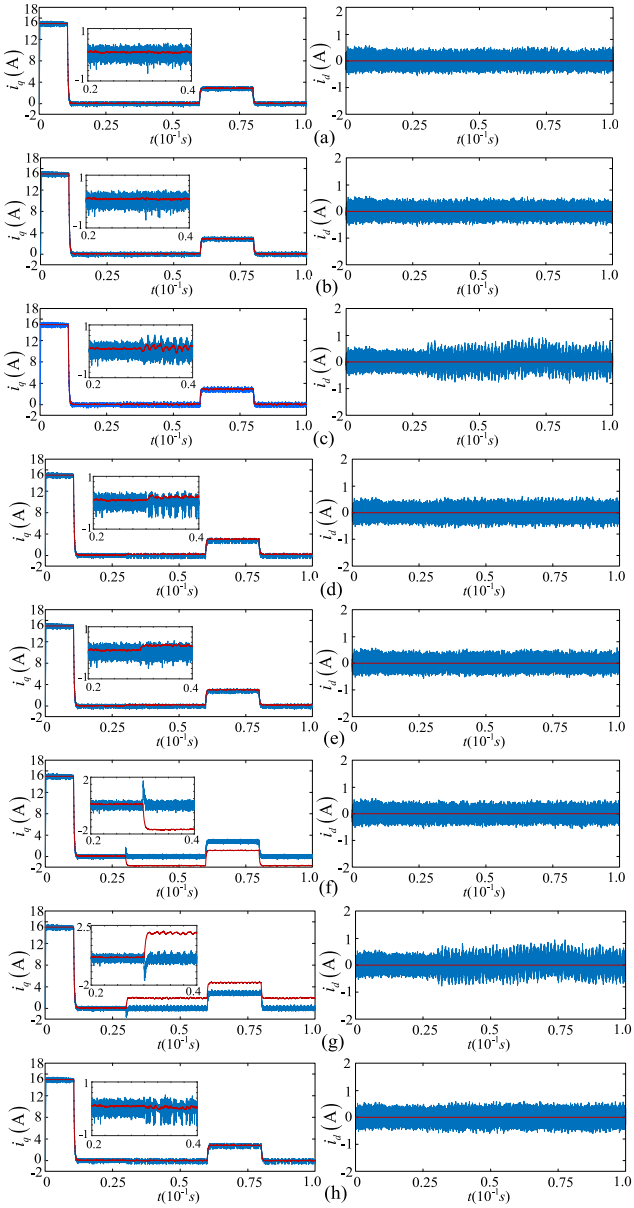

Fig. 7. Simulation performance of the conventional DBPC method under different parameter mismatch conditions. (a) $\Delta R_s = -0.9R_s$. (b) $\Delta R_s = 9R_s$. (c) $\Delta L_s = -0.9L_s$. (d) $\Delta L_s = 9L_s$. (e) $\Delta\psi_f = -0.9\psi_f$. (f) $\Delta\psi_f = 9\psi_f$. (g) $\Delta R_s = -0.9R_s$, $\Delta L_s = -0.9L_s$, and $\Delta\psi_f = -0.9\psi_f$. (h) $\Delta R_s = 9R_s$, $\Delta L_s = 9L_s$, and $\Delta\psi_f = 9\psi_f$.

The parameters of the composite SMDO are $g_1 = 72\,000$, $g_2 = 72\,000$, and $g_3 = 48\,000$, which ensure the asymptotic stability of composite SMDO. The speed reference is set as 360 r/min, and the sampling frequency used in the simulation and experiment is 50 kHz, while the external loop sampling frequency is 5 kHz. At the time instants $t_1 = 0.06$ s and $t_2 = 0.08$ s, step changes in the load torque from 0 to 20 N·m and from 20 to 0 N·m have been applied to the system, respectively. Parameter variations are set at 0.03 s to show the simulation results.

Under different parameter mismatch conditions, the simulation results of the *dq* axes current responses and current references are shown in Figs. 7 and 8. The blue line is the

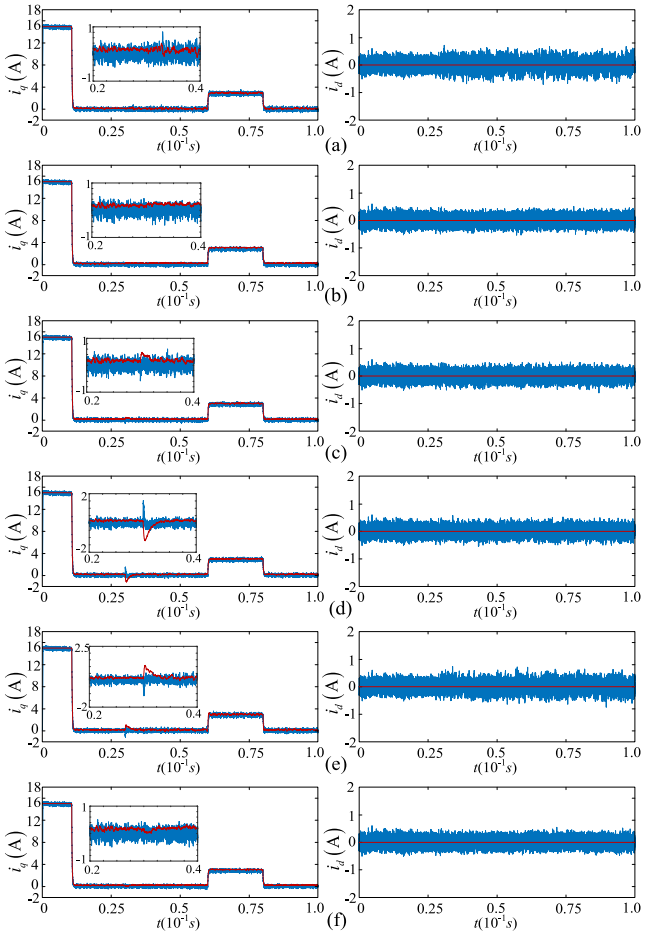

Fig. 8. Simulation performance of the proposed DBPC method under different parameter mismatch conditions. (a) $\Delta L_s = -0.9L_s$. (b) $\Delta L_s = 9L_s$. (c) $\Delta\psi_f = -0.9\psi_f$. (d) $\Delta\psi_f = 9\psi_f$. (e) $\Delta R_s = -0.9R_s$, $\Delta L_s = -0.9L_s$, and $\Delta\psi_f = -0.9\psi_f$. (f) $\Delta R_s = 9R_s$, $\Delta L_s = 9L_s$, and $\Delta\psi_f = 9\psi_f$.

current response, while the brown line is the current reference. In Fig. 7, the simulation results of the conventional DBPC are illustrated. It is seen that the parameter mismatch of inductance L_s and flux linkage ψ_f produces great influence on the dq axes current responses. In contrast, the variation of resistance R_s has little effect on current response when the other parameters remain unchanged, which is similar to the parameter sensitivity analysis in Section III. Furthermore, different parameter variations cause current response error, which can be calculated by (11). Additionally, Fig. 8 presents the simulation results of the proposed DBPC method with compensation voltage based on the composite SMDO, which can exactly track the current references under parameters mismatch compared with the traditional strategy.

Fig. 9 shows the compensation voltages of the proposed DBPC method under different parameter mismatch conditions, respectively. The blue line is the d-axis current compensation voltage, while the red line is the q-axis compensation voltage. Due to the little effect of resistance variation ΔR_s on current responses, the parameter mismatch of resistance R_s is not studied in the following analysis. As shown in Fig. 9, compensation

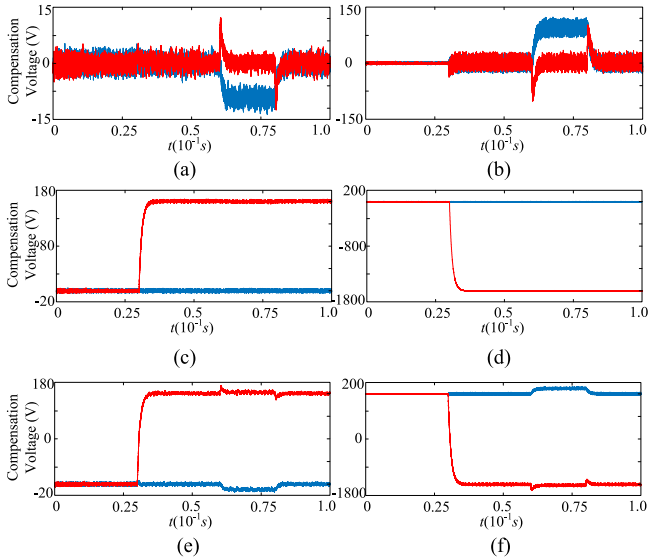

Fig. 9. Compensation voltage of the proposed DBPC method under different parameter mismatch conditions. (a) $\Delta L_s = -0.9L_s$. (b) $\Delta L_s = 9L_s$. (c) $\Delta\psi_f = -0.9\psi_f$. (d) $\Delta\psi_f = 9\psi_f$. (e) $\Delta R_s = -0.9R_s$, $\Delta L_s = -0.9L_s$, and $\Delta\psi_f = -0.9\psi_f$. (f) $\Delta R_s = 9R_s$, $\Delta L_s = 9L_s$, and $\Delta\psi_f = 9\psi_f$.

voltages are produced to eliminate the influence of parameters variation when parameter mismatch exists after 0.03 s. Furthermore, compensation voltage is related to load torque because the variation of load torque causes current response to change, which further affects the compensation voltage in parameter mismatch condition.

The control system is implemented on a dSPACE 1401 real-time platform with a control desk. The rapid control prototype is realized based on the dSPACE. The experimentally measured currents are available via an analog-to-digital converter board. The experimental results are shown in Figs. 10–13. The parameter mismatch is set at 0.05 s. At the time instants $t_1 = 0.1$ s and $t_2 = 0.15$ s, step changes in the load torque from 0 to 20 N·m and from 20 to 0 N·m are applied to the system, respectively.

As shown in Fig. 10, the reference currents have a step change and the ripple of currents response becomes larger when the parameter mismatch exists at 0.05 s. In particular, the variation of permanent flux produces significant effect on currents response, which results in the q-axis current error of 1.8 A. Furthermore, when three parameters variation exists simultaneously, the q-axis current of the conventional DBPC fails to track the reference value accurately with an error of about 2 A, while the d-axis current response produces large fluctuations of 1.6 A, thanks to the coupling in a motor model.

Compared with the conventional method, the currents tracking error is smaller except for the acceptable ripple at the original instant of parameter mismatch. In Fig. 11(b) and (c), the transient ripples of the current response are about -1.2 and 0.9 A, respectively, which converge to stable reference values quickly. Meanwhile, the compensation voltages are given in Fig. 12, which are used to eliminate the influence of parameter mismatch. Different parameter mismatch conditions cause different

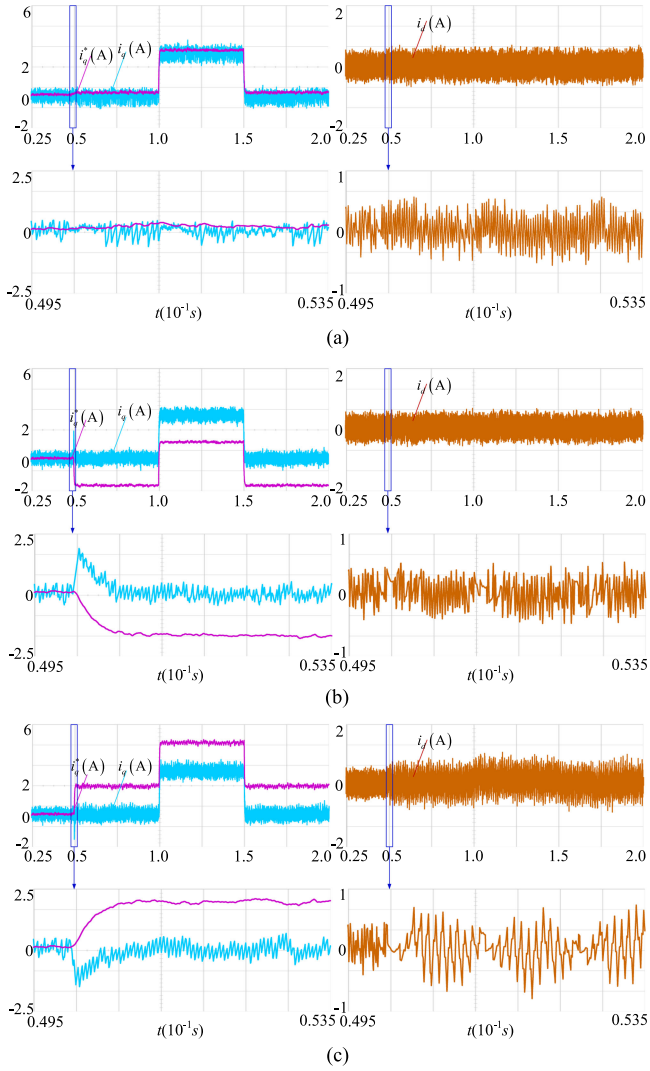

Fig. 10. Experimental results of the conventional DBPC method. (a) $\Delta L_s = 9L_s$. (b) $\Delta\psi_f = 9\psi_f$. (c) $\Delta R_s = -0.9R_s$, $\Delta L_s = -0.9L_s$, and $\Delta\psi_f = -0.9\psi_f$.

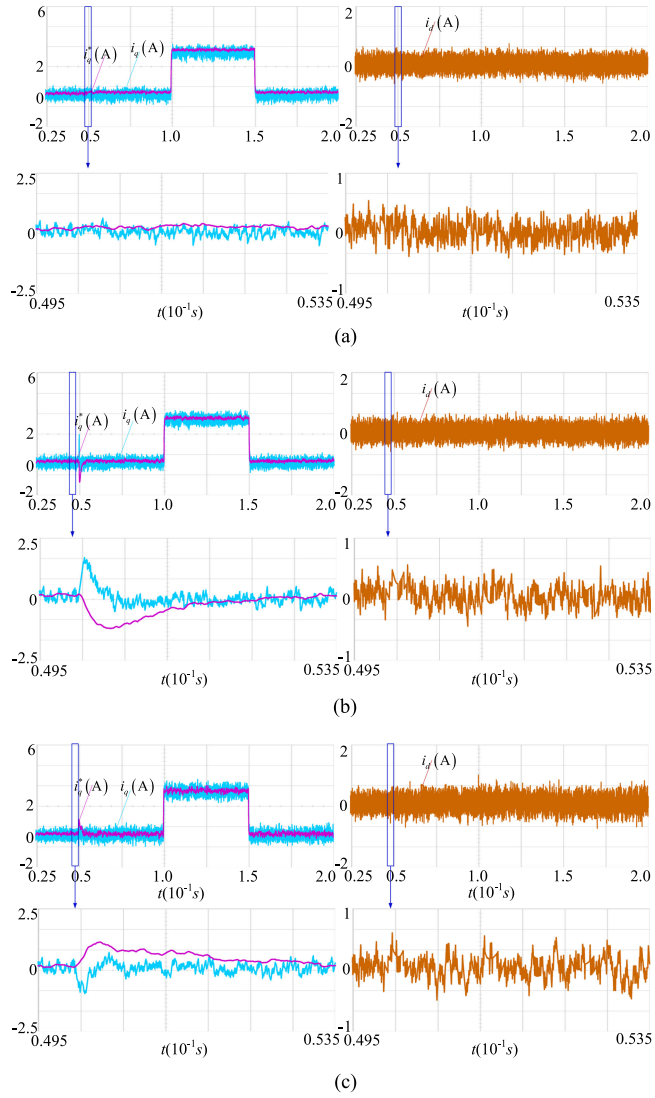

Fig. 11. Experimental results of the proposed DBPC method. (a) $\Delta L_s = 9L_s$. (b) $\Delta\psi_f = 9\psi_f$. (c) $\Delta R_s = -0.9R_s$, $\Delta L_s = -0.9L_s$, and $\Delta\psi_f = -0.9\psi_f$.

perturbance, which results in different voltage compensations, according to (6) and (13).

Fig. 13 illustrates the control performance of both methods when three parameters mismatch occurs during operation in which step changes in the reference speed from 360 to 365 r/min and from 365 to 360 r/min have been applied at 0.1 and 0.15 s, respectively. Under the conventional predictive control method, the existing parameters mismatch affects the current response and produces the permanent q-axis current tracking error of 4.8 A and the d-axis current fluctuation of 1.1 A, which deteriorates the control performance. Compared with the conventional method, the proposed DBPC method produces obvious current errors only at 0.05, 0.1, and 0.15 s, which converges to stable reference quickly. Therefore, the improved method ensures that the control performance is not subject to parameter variation. The ripples and errors of the current response can be suppressed effectively.

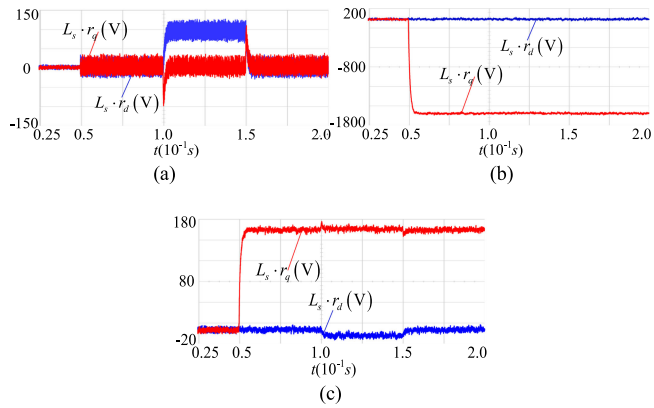

Fig. 12. Compensation voltage of the proposed DBPC method. (a) $\Delta L_s = 9L_s$. (b) $\Delta\psi_f = 9\psi_f$. (c) $\Delta R_s = -0.9R_s$, $\Delta L_s = -0.9L_s$, and $\Delta\psi_f = -0.9\psi_f$.

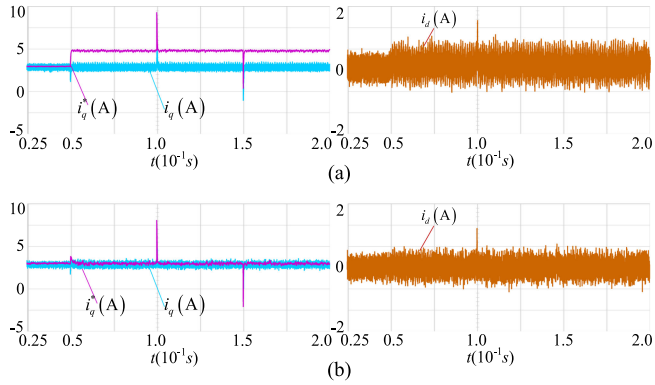

Fig. 13. Experimental results in reference speed step-change conditions. (a) Conventional DBPC method. (b) Proposed DBPC method.

VI. Conclusion

In this article, an improved DB predictive current controller was proposed and experimentally applied to a PMSM drive system to enhance the robust performance of the drive system. In order to evaluate the relationship between the current response and mismatch of three parameters, the parameter sensitivity analysis was discussed first. Then, an SMDO based on the stator current and lumped disturbance was designed to simultaneously estimate the future current value and lumped disturbance caused by the parameter mismatch, which can effectively eliminate the influence of parameters mismatch. Furthermore, considering the influence of the calculation and sampling delay, currents are estimated by the discrete expression of composite SMDO and used to replace the sampled values to compensate one-step delay.

Compared with the related references, which adopt a high-order sliding-mode structure or new reaching law-based method, this design method based on the state-space structure of the control plant reduced the calculation complexity of the observation value for the nonlinear model. Additionally, the second-order expansion of the rotor speed was applied to improve the current reference accuracy. The simulation and experimental results confirmed the performance of the proposed control strategy.

In future work, the composite observation system will be further studied, which comprehensively considers the variation of mechanical parameters. Meanwhile, the balance of calculation burden and control performance will be considered.

References

[1] Z. Shi, X. Sun, Y. Cai, and Z. Yang, "Robust design optimization of a five-phase PM hub motor for fault-tolerant operation based on Taguchi method," *IEEE Trans. Energy Convers.*, vol. 35, no. 4, pp. 2036–2044. Dec. 2020.

[2] X. Sun, C. Hu, G. Lei, Y. Guo, and J. Zhu, "State feedback control for a PM hub motor based on grey wolf optimization algorithm," *IEEE Trans. Power Electron.*, vol. 35, no. 1, pp. 1136–1146, Jan. 2020.

[3] X. Sun, Z. Shi, G. Lei, Y. Guo, and J. Zhu, "Multi-objective design optimization of an IPMSM based on multilevel strategy," *IEEE Trans. Ind. Electron.*, vol. 68, no. 1, pp. 139–148, Jan. 2021.

[4] W. Hu, C. Ruan, H. Nian, and D. Sun, "An improved modulation technique with minimum switching actions within one PWM cycle for open-end winding PMSM system with isolated DC bus," *IEEE Trans. Ind. Electron.*, vol. 67, no. 5, pp. 4259–4264, May 2020.

[5] X. Sun, J. Cao, G. Lei, Y. Guo, and J. Zhu, "Speed sensorless control for permanent magnet synchronous motors based on finite position set," *IEEE Trans. Ind. Electron.*, vol. 67, no. 7, pp. 6089–6100, Jul. 2020.

[6] S. Li and Z. Liu, "Adaptive speed control for permanent-magnet synchronous motor system with variations of load inertia," *IEEE Trans. Ind. Electron.*, vol. 56, no. 8, pp. 3050–3059, Aug. 2009.

[7] X. Sun, Z. Jin, Y. Cai, Z. Yang, and L. Chen, "Grey wolf optimization algorithm based state feedback control for a bearingless permanent magnet synchronous machine," *IEEE Trans. Power Electron.*, vol. 35, no. 12, pp. 13631–13640, Dec. 2020.

[8] J. Hang, J. Zhang, M. Xia, S. Ding, and W. Hua, "Interturn fault diagnosis for model-predictive-controlled-PMSM based on cost function and wavelet transform," *IEEE Trans. Power Electron.*, vol. 35, no. 6, pp. 6405–6418, Jun. 2020.

[9] D. Casadei, F. Profumo, G. Serra, and A. Tani, "FOC and DTC: Two viable schemes for induction motors torque control," *IEEE Trans. Power Electron.*, vol. 17, no. 5, pp. 779–787, Sep. 2002.

[10] L. Malesani, P. Mattavelli, and P. Tomasin, "Improved constant-frequency hysteresis current control of VSI inverters with simple feedforward bandwidth prediction," *IEEE Trans. Ind. Appl.*, vol. 33, no. 5, pp. 1194–1202, Sep./Oct. 1997.

[11] O. Sandre-Hernandez, J. Rangel-Magdaleno, and R. Morales-Caporal, "A comparison on finite-set model predictive torque control schemes for PMSMs," *IEEE Trans. Power Electron.*, vol. 33, no. 10, pp. 8838–8847, Oct. 2018.

[12] M. Wu, X. Sun, J. Zhu, G. Lei, and Y. Guo, "Improved model predictive torque control for PMSM drives based on duty cycle optimization," *IEEE Trans. Magn.*, vol. 57, no. 2, Feb. 2021, Art. no. 8200505.

[13] W. Tu, G. Luo, Z. Chen, L. Cui, and R. Kennel, "Predictive cascaded speed and current control for PMSM drives with multi-timescale optimization," *IEEE Trans. Power Electron.*, vol. 34, no. 11, pp. 11046–11061, Nov. 2019.

[14] P. Kakosimos and H. Abu-Rub, "Predictive speed control with short prediction horizon for permanent magnet synchronous motor drives," *IEEE Trans. Power Electron.*, vol. 33, no. 3, pp. 2740–2750, Mar. 2018.

[15] X. Sun *et al.*, "MPTC for PMSMs of EVs with multi-motor driven system considering optimal energy allocation," *IEEE Trans. Magn.*, vol. 55, no. 7, Jul. 2019, Art. no. 8104306.

[16] M. Siami, D. A. Khaburi, M. Rivera, and J. Rodríguez, "An experimental evaluation of predictive current control and predictive torque control for a PMSM fed by a matrix converter," *IEEE Trans. Ind. Electron.*, vol. 64, no. 11, pp. 8459–8471, Nov. 2017.

[17] J. Rodriguez *et al.*, "State of the art of finite control set model predictive control in power electronics," *IEEE Trans. Ind. Inform.*, vol. 9, no. 2, pp. 1003–1016, May 2013.

[18] L. Rovere, A. Formentini, A. Gaeta, P. Zanchetta, and M. Marchesoni, "Sensorless finite-control set model predictive control for IPMSM drives," *IEEE Trans. Ind. Electron.*, vol. 63, no. 9, pp. 5921–5931, Sep. 2016.

[19] T. Trker, U. Buyukkeles, and A. F. Bakan, "A robust predictive current controller for PMSM drives," *IEEE Trans. Ind. Electron.*, vol. 63, no. 6, pp. 3906–3914, Jun. 2016.

[20] X. Sun, L. Chen, Z. Yang, and H. Zhu, "Speed-sensorless vector control of a bearingless induction motor with artificial neural network inverse speed observer," *IEEE/ASME Trans. Mechatronics*, vol. 18, no. 4, pp. 1357–1366, Aug. 2013.

[21] Y. A.-R. I. Mohamed and E. F. El-Saadany, "Robust high bandwidth discrete-time predictive current control with predictive internal model: A unified approach for voltage-source PWM converters," *IEEE Trans. Power Electron.*, vol. 23, no. 1, pp. 126–136, Jan. 2008.

[22] L. Chen, H. Xu, X. Sun, and Y. Cai, "Three-vector-based model predictive torque control for a permanent magnet synchronous motor of EVs," *IEEE Trans. Transp. Electrific.*, to be published, doi: 10.1109/TTE.2021.3053256.

[23] L. Malesani, P. Mattavelli, and S. Buso, "Robust dead-beat current control for PWM rectifiers and active filters," *IEEE Trans. Ind. Appl.*, vol. 35, no. 3, pp. 613–620, May/Jun. 1999.

[24] H.-T. Moon, H.-S. Kim, and M.-J. Youn, "A discrete-time predictive current control for PMSM," *IEEE Trans. Power Electron.*, vol. 18, no. 1, pp. 464–472, Jan. 2003.

[25] H. Liu and S. Li, "Speed control for PMSM servo system using predictive functional control and extended state observer," *IEEE Trans. Ind. Electron.*, vol. 59, no. 2, pp. 1171–1183, Feb. 2012.

[26] X. Sun, M. Wu, G. Lei, Y. Guo, and J. Zhu, "An improved model predictive current control for PMSM drives based on current track circle," *IEEE Trans. Ind. Electron.*, vol. 68, no. 5, pp. 3782–3793, May 2021.

[27] X. Sun, Z. Shi, G. Lei, Y. Guo, and J. Zhu, "Analysis and design optimization of a permanent magnet synchronous motor for a campus patrol electric vehicle," *IEEE Trans. Veh. Technol.*, vol. 68, no. 11, pp. 10535–10544, Nov. 2019.
[28] X. Lin, W. Huang, W. Jiang, Y. Zhao, and S. Zhu, "Deadbeat direct torque and flux control for permanent magnet synchronous motor based on stator flux oriented," *IEEE Trans. Power Electron.*, vol. 35, no. 5, pp. 5078–5092, May 2020.
[29] A. M. Aljehaimi and P. Pillay, "Novel flux linkage estimation algorithm for a variable flux PMSM," *IEEE Trans. Ind. Appl.*, vol. 54, no. 3, pp. 2319–2335, May/Jun. 2018.
[30] X. Zhang, B. Hou, and Y. Mei, "Deadbeat predictive current control of permanent-magnet synchronous motors with stator current and disturbance observer," *IEEE Trans. Power Electron.*, vol. 32, no. 5, pp. 3818–3834, May 2017.
[31] L. Tong *et al.*, "An SRF-PLL-based sensorless vector control using the predictive deadbeat algorithm for the direct-driven permanent magnet synchronous generator," *IEEE Trans. Power Electron.*, vol. 29, no. 6, pp. 2837–2849, Jun. 2014.
[32] L. Rovere, A. Formentini, and P. Zanchetta, "FPGA implementation of a novel oversampling deadbeat controller for PMSM drives," *IEEE Trans. Power Electron.*, vol. 66, no. 5, pp. 3731–3741, May 2019.
[33] P. Wipasuramonton, Z. Q. Zhu, and D. Howe, "Predictive current control with current-error correction for PM brushless AC drives," *IEEE Trans. Ind. Appl.*, vol. 42, no. 4, pp. 1071–1079, Jul./Aug. 2006.
[34] Y. Jiang, W. Xu, C. Mu, and Y. Liu, "Improved deadbeat predictive current control combined sliding mode strategy for PMSM drive system," *IEEE Trans. Veh. Technol.*, vol. 67, no. 1, pp. 251–263, Jan. 2018.

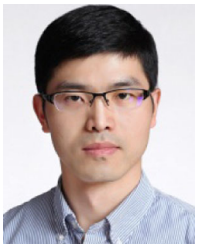

Xiaodong Sun (Senior Member, IEEE) received the B.Sc. degree in electrical engineering and the M.Sc. and Ph.D. degrees in control engineering from Jiangsu University, Zhenjiang, China, in 2004, 2008, and 2011, respectively.

Since 2004, he has been with Automotive Engineering Research Institute, Jiangsu University, where he is currently a Professor of vehicle engineering. From 2014 to 2015, he was a Visiting Professor with the School of Electrical, Mechanical, and Mechatronic Systems, University of Technology Sydney, Sydney, NSW, Australia. His current teaching and research interests include electrified vehicles, electrical machines, electrical drives, and energy management. He is the author or co-author of more than 100 refereed technical papers and one book, and the holder of 42 patents in his areas of interest.

Dr. Sun is an Editor for the IEEE TRANSACTIONS ON ENERGY CONVERSION.

Junhao Cao was born in Huaian, Jiangsu, China, in 1994. He received the B.S. degree in vehicle engineering in 2018 from Jiangsu University, Zhenjiang, China, where he is currently working toward the M.E. degree in vehicle engineering.

His current research interests include control of electrical drive systems and advanced control strategy of an electric machine.

Gang Lei (Member, IEEE) received the B.S. degree in mathematics from Huanggang Normal University, Huanggang, China, in 2003, and the M.S. degree in mathematics and the Ph.D. degree in electrical engineering from the Huazhong University of Science and Technology, Wuhan, China, in 2006 and 2009, respectively.

He is currently a Senior Lecturer in electrical engineering with the School of Electrical and Data Engineering, University of Technology Sydney, Sydney, NSW, Australia. His research interests focus on design optimization and control of electrical drive systems and renewable energy systems.

Dr. Lei is an Associate Editor for the IEEE TRANSACTIONS ON INDUSTRIAL ELECTRONICS and an Editor for the IEEE TRANSACTIONS ON ENERGY CONVERSION.

Youguang Guo (Senior Member, IEEE) received the B.E. degree from the Huazhong University of Science and Technology, Wuhan, China, in 1985, the M.E. degree from Zhejiang University, Hangzhou, China, in 1988, and the Ph.D. degree from the University of Technology Sydney (UTS), Sydney, NSW, Australia, in 2004, all in electrical engineering.

He is currently an Associate Professor of electrical engineering with the School of Electrical and Data Engineering, UTS. His research interests include measurement and modeling of properties of magnetic materials, numerical analysis of the electromagnetic field, electrical machine design optimization, and power electronic drives and control.

Jianguo Zhu (Senior Member, IEEE) received the B.E. degree from the Jiangsu Institute of Technology, Zhenjiang, China, in 1982, the M.E. degree from the Shanghai University of Technology, Shanghai, China, in 1987, and the Ph.D. degree from the University of Technology Sydney (UTS), Sydney, NSW, Australia, in 1995, all in electrical engineering.

He was a Lecturer in 1994, a Full Professor in 2004, and a Distinguished Professor of electrical engineering in 2017 with UTS, where he has held various leadership positions, including the Head of the School of Electrical, Mechanical, and Mechatronic Systems and the Director of the Centre of Electrical Machines and Power Electronics. In 2018, he joined the University of Sydney, Australia, as a Full Professor and the Head of the School of Electrical and Information Engineering. His research interests include computational electromagnetics, measurement and modeling of magnetic properties of materials, electrical machines and drives, power electronics, renewable energy systems, and smart microgrids.